Thin film reaction of transition metals with germanium

S. Gaudet[a)]
Regroupement Québécois sur les Matériaux de Pointe (RQMP), École Polytechnique de Montréal, P.O. Box 6079, Station Centre-Ville, Montréal, Québec H3C 3A7, Canada and Département de Génie Physique, École Polytechnique de Montréal, P.O. Box 6079, Station Centre-Ville, Montréal, Québec H3C 3A7, Canada

C. Detavernier
Department of Solid State Physics, Ghent University, Ghent 9000, Belgium

A. J. Kellock
IBM Almaden Research Center, 650 Harry Road, San Jose, California 95120

P. Desjardins
Regroupement Québécois sur les Matériaux de Pointe (RQMP), École Polytechnique de Montréal, P.O. Box 6079, Station Centre-Ville, Montréal, Québec H3C 3A7, Canada and Département de Génie Physique, École Polytechnique de Montréal, P.O. Box 6079, Station Centre-Ville, Montréal, Québec H3C 3A7, Canada

C. Lavoie
IBM T.J. Watson Research Center, Yorktown Heights, New York 10598 and Département de Génie Physique, École Polytechnique de Montréal, Montréal, Québec H3C 3A7, Canada

(Received 16 December 2005; accepted 7 March 2006; published 20 April 2006)

A systematic study of the thermally induced reaction of 20 transition metals (Ti, Zr, Hf, V, Nb, Ta, Cr, Mo, W, Mn, Re, Fe, Ru, Co, Rh, Ir, Ni, Pd, Pt, and Cu) with Ge substrates was carried out in order to identify appropriate contact materials in Ge-based microelectronic circuits. Thin metal films, nominally 30 nm thick, were sputter deposited on both amorphous Ge and crystalline Ge(001). Metal-Ge reactions were monitored *in situ* during ramp anneals at 3 °C s^{-1} in an atmosphere of purified He using time-resolved x-ray diffraction, diffuse light scattering, and resistance measurements. These analyses allowed the determination of the phase formation sequence for each metal-Ge system and the identification of the most promising candidates—in terms of sheet resistance and surface roughness—for their use as first level interconnections in microelectronic circuits. A first group of metals (Ti, Zr, Hf, V, Nb, and Ta) reacted with Ge only at temperatures well above 450 °C and was prone to oxidation. Another set (Cr, Mo, Mn, Re, Rh, Ru, and Ir) did not form low resistivity phases ($<130\ \mu\Omega$ cm) whereas no reaction was observed in the case of W even after annealing at up to 1000 °C. We found that Fe, Co, Ni, Pd, Pt, and Cu were the most interesting candidates for microelectronic applications as they reacted at relatively low temperatures (150–360 °C) to form low resistivity phases (22–129 $\mu\Omega$ cm). Among those, two monogermanides, NiGe and PdGe, exhibited the lowest resistivity values (22–30 $\mu\Omega$ cm) and were stable over the widest temperature window during ramp anneals. In passing, we note that Cu, Ni, and Pd were the most effective in lowering the crystallization temperature of amorphous Ge, by up to 290 °C for our typical ramp anneals at 3 °C s^{-1}. © *2006 American Vacuum Society.*
[DOI: 10.1116/1.2191861]

I. INTRODUCTION

Microelectronics has been primarily a Si-based technology because of the stability and high quality of SiO_2 and its interface with the Si substrate, as well as the enormous investment made in Si processing and device fabrication. We expect, however, to witness major changes in the coming years. First, strained $Si_{1-x}Ge_x$ layers with adjustable band gaps, large valence band offsets, and high carrier mobilities have been used to develop high-speed heterojunction bipolar transistors (HBTs),[1,2] modulation-doped Si–Ge *p*-type metal-oxide-semiconductor field-effect transistors (MOSFETs),[2,3] and quantum effect (including Coulomb blockade) devices.[4,5] Si–Ge *n*- and *p*-type modulation-doped field effect transistors (MODFETs) with switching times comparable to those obtained with III–V semiconductors have also been reported.[6] Second, the replacement of SiO_2 as the preferred gate insulator in MOSFET devices by new high-dielectric constant materials required for the continued scaling of device dimensions[7] has for consequence to eliminate one of the strongest advantages of silicon as the active material, its remarkable oxide not being used as the gate insulator anymore. A variety of alternate semiconducting materials exhibiting higher mobilities thus becomes appealing alternatives for replacing the silicon active region. Because of its higher carrier mobilities[8] and relative compatibility with silicon processing, Ge is often proposed as a potential alternative.

[a)]Electronic mail: simon.gaudet@polymtl.ca

Page 1 of 12 TSMC EXHIBIT 1055

As the possibility of using Ge in microelectronics arises, developing optimal contact materials becomes of paramount importance. In analogy with the current Si-based technology, where metal silicides are used to contact the source, drain, and gate of the transistors, metal germanides appear as natural candidates for contacting Ge. In the current design and processing of transistors, the contact material should exhibit low sheet and contact resistances, good stability under heat treatment, and be formed at low temperature. From a device processing point of view, it is also important to determine the exact phase sequence occurring during the annealing of thin metal films on Ge in order to establish the temperature range over which a phase may be of use in the industry.

Most work on *bulk* germanides has been carried out before 1970. It has been compiled by Samsonov and Bondarev in a book presenting the various phases observed for each materials system as well their melting and superconducting transition temperatures.[9] Formation enthalpies and resistivity values are also presented for selected materials. The phase diagrams are also available for all systems investigated here but Ta–Ge and Ir–Ge.[10]

Data on thin film systems are relatively scarce, a phase formation sequence having been proposed for only 11 of the 20 systems considered here.[11–30] In all previous investigations, the phase sequence has been determined through anneal-and-quench experiments with typical temperature intervals of 25–100 °C. The observed phase sequence generally begins with metal-rich phases and evolves towards the phase containing the largest Ge fraction. A number of thermodynamically stable phases have not been observed in these experiments. Furthermore, the nature of the substrate, the film thickness, the deposition technique, and the temperature ramp rate vary significantly in each of these experiments, making detailed comparisons very difficult.

Since $TiSi_2$, $CoSi_2$, and NiSi are used in the current silicon-based technology, interest has arisen for their corresponding germanides. Several different phase sequences have been reported for Ti–Ge.[11–14] The common denominator is that the low resistivity phase, $TiGe_2$, forms at relatively high temperature (800 °C) and shows a resistivity of 20 $\mu\Omega$ cm.[11–14] Investigations of Co–Ge reactions revealed different first phases with the reaction ending with $CoGe_2$ in all cases. This phase appears at 425 °C and is characterized by a resistivity of 35 $\mu\Omega$ cm.[15–18] Two studies have proposed that the Ni–Ge phase sequence is Ni_2Ge, NiGe while another suggests Ni_5Ge_3 followed by NiGe.[14,16,19–21] NiGe has a low resistivity (16 $\mu\Omega$ cm), and forms, but also degrades, at relatively low temperatures (400 and 550 °C, respectively). These trends for the formation temperature of the low resistivity phases are similar to those observed for the corresponding silicides.

The reactions of germanium with Pd,[14,16,22,23] Pt,[14,24,25] Hf,[16] Ta,[14,26] Cr,[27,28] Mn,[16] Rh,[16] and Cu (Refs. 29 and 30) have also been investigated. In three of these systems, a single phase has been reported to form, namely, Hf_5Ge_3, $TaGe_2$, and Mn_5Ge_3. In other cases, a limited number of investigations identified the consecutive appearance of two phase: RhGe and $Rh_{17}Ge_{22}$ for the Rh–Ge couple, Pd_2Ge and PdGe for Pd–Ge, and Cu_3Ge (monoclinic) and Cu_3Ge (hexagonal) for Cu–Ge. The situation is more complex for the Pt–Ge system with various sequences each involving four phases having been published. While the first phase to appear is either Pt_3Ge_2 or Pt_2Ge depending on the investigation considered, there is a consensus on the subsequent sequence: PtGe, Pt_2Ge_3, and $PtGe_2$.[14,15,25] No data on the reaction of Zr, V, Nb, Mo, W, Re, Fe, Ru, and Ir thin films with Ge have been previously reported in the literature.

We note that the observation of different phase sequences for the same materials system is likely due to differences in film thicknesses and microstructure, and in annealing conditions. Moreover, it is possible that a phase that is present for only a very small temperature window during annealing could be inadvertently missed in the anneal-and-quench experiments summarized above since temperature intervals are typically greater than 25 °C.

In this work, we report on a systematic study of the solid-state reaction between thin metal films and Ge in which we determined the phase formation sequence and film properties of most transition metal germanides. Metal-Ge reactions were monitored *in situ* during ramp anneals using time-resolved x-ray diffraction (XRD), diffuse light scattering, and resistance measurements. We found that Fe, Co, Ni, Pd, Pt, and Cu were the most interesting candidates for microelectronics applications as they reacted at relatively low temperatures (150–360 °C) to form low resistivity phases (22–129 $\mu\Omega$ cm). Among those, two monogermanides, NiGe and PdGe, exhibited the lowest resistivity (22–30 $\mu\Omega$ cm) and were stable over the widest temperature window during ramp anneals.

II. EXPERIMENTAL PROCEDURE

Blanket films, nominally 30 nm thick, of 20 transition metals—Ti, Zr, Hf, V, Nb, Ta, Cr, Mo, W, Mn, Re, Fe, Ru, Co, Rh, Ir, Ni, Pd, Pt, and Cu—were deposited at room temperature by magnetron sputtering on three different substrates: (i) Ge(001), (ii) 200 nm amorphous germanium (α-Ge) on 100 nm SiO_2/Si(001), and (iii) 50 nm Si_3N_4 on Si(001). As described below, the latter inert substrate was used to determine whether the metal films were prone to oxidation. Prior to deposition, the Ge substrates were cleaned with dilute HF (100:1). No additional cleaning steps were used prior to metal deposition on the freshly grown Si_3N_4 layers.

The base vacuum of the magnetron sputtering system was 1×10^{-9} Torr (1.3×10^{-7} Pa) and the Ar pressure during deposition was maintained at 4 mTorr (0.53 Pa). The deposition rates ranged from 0.04 to 0.32 nm s^{-1} depending on the nature of the metal target. A second series of samples on Ge(001) and α-Ge substrates was subject to the same metal depositions but the samples were immediately capped—without breaking vacuum—with a 5-nm-thick α-Ge layer in order to prevent oxidation.

Metal-Ge reactions were monitored *in situ* during ramp anneals in a purified He atmosphere using time-resolved

XRD, diffuse light scattering, and resistance measurements.

These measurements were performed at the X20C beamline of the National Synchrotron Light Source (NSLS) at Brookhaven National Laboratory. As-deposited samples were mounted in an annealing chamber aligned along the beamline and equipped with an x-ray-transparent Be window. The chamber was evacuated to 5×10^{-6} Torr (7×10^{-4} Pa), backfilled with purified He ($O_2<10^{-7}$ ppm), reevacuated, and then backfilled with 1 atm of He. As-deposited samples were annealed using linear temperature ramps from 100 to 900 °C at 3 °C s^{-1}. Substrate temperatures are measured with a thermocouple and calibrated to better than ±3 °C using the Si–Au, Si–Al, and Si–Ag eutectic melting points measured on a Si(001) substrate. A high-intensity monochromator employing bandpass W–Si multilayer filters provides an energy resolution of 1.5% at 6.9 keV ($\lambda=0.1797$ nm) with a typical intensity at the sample of 3×10^{13} photons s^{-1}. The incident x rays illuminated a sample area of 1×2 mm^2. Each diffraction curve was collected with an acquisition time ranging from 0.5 to 2 s using a position-sensitive detector covering a 2θ range of 14°. *In situ* light scattering measurements were carried out using a He–Ne laser light with a wavelength of 633 nm at an incidence angle of 65° with respect to the surface normal and scattering angles of −20° and 50° (with two separate detectors) providing information on changes in surface roughness for in-plane correlation lengths of 0.5 and 5 μm, respectively. Changes in sample resistance during annealing were measured *in situ* using standard four point probe geometry.

Ex situ electrical measurements using a four point probe were performed on quenched samples to determine their sheet resistance at room temperature. Rutherford backscattering spectroscopy (RBS) measurements were carried out to confirm the composition of all as-deposited films, and of selected quenched samples to corroborate phase identification. The RBS probe beam consisted of 2.3 MeV $^4He^+$ ions incident at an angle of 7° relative to the sample surface normal. Scattered ions were collected at two differents angles, 170° to better separate the Ni and Ge signals and 95° for better depth resolution. RBS also confirmed that there was no interaction between the Ge and the other metal in the as-deposited case and that all interfaces were flat and continuous with an average rms roughness <3 nm. Simulations of multiphased layer stacks were then carried out using the RUMP software package.[31] The deposited films were also characterized on carbon pieces to minimize the contribution of the substrate, in order to verify by RBS that the as-deposited films were oxygen-free. No impurities could be detected by RBS in the as-deposited samples.

III. RESULTS

All as-deposited samples were annealed using linear temperature ramps in order to study the phase formation sequence, to identify low resistivity phases, and to determine sensitivity to oxidation. The experimental matrix being considerable (20 different metals with substrates), the presentation of the results will emphasize the main differences between the various materials systems. However, in order to demonstrate the strength and rigor of our experimental approach we first present the detailed *in situ* results for a typical system, Pt–Ge.

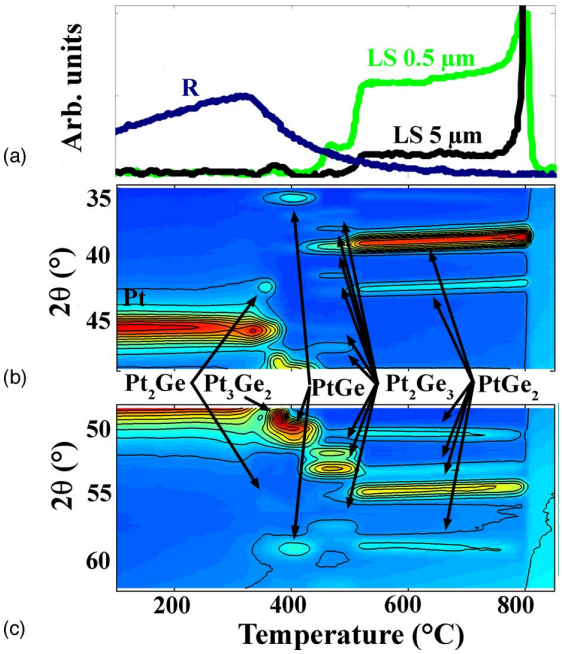

FIG. 1. (a) Resistance (R) and light scattering (LS) signals and [(b) and (c)] XRD intensity contour maps ($\lambda=0.1797$ nm, log scale intensity) plotted as a function of annealing temperature T_a during a thermal ramp at 3 °C s^{-1} in purified He for a 30-nm-thick Pt layer deposited on Ge(001). LS 0.5 μm and LS 5 μm correspond to the light scattering intensity signals measured at angles selected to probe surface roughness variations for in-plane correlation lengths of 0.5 and 5 μm, respectively.

The reaction of a 30-nm-thick Pt layer on a Ge(001) substrate, a system that exhibits a significant number of phase transitions, has been followed during thermal ramping from room temperature to 900 °C at 3 °C s^{-1}. Figure 1 shows two contour plots of the logarithm of the scattered synchrotron x-ray intensity as a function of diffraction angle 2θ and annealing temperature T_a. Since the angular range of the position-sensitive detector for the synchrotron measurements is limited to 14°, the two plots represent two consecutive measurements on nominally identical samples and covering different 2θ windows. They are both presented in order to include all relevant peaks from the Pt–Ge system. The diffuse light scattering data plotted in Fig. 1(a) is useful in revealing subtle film transformations that might not be visible in the x-ray diffraction signal. The *in situ* resistance data are, in the present case, dominated by the behavior of the thick Ge(001) substrate.

The data in Fig. 1 clearly indicate that only the Pt(111) peak at $2\theta_{Pt(111)}=46.7°$ is visible at the beginning of the annealing treatment. Several abrupt, consecutive phase transitions are detected by XRD. We identify the formation of the metal-rich phase Pt_2Ge at $T_a=330$ °C on the basis of its (111) and (003) peaks at $2\theta=43.0°$ and 57.8°, respectively. Both light scattering signals (0.5 and 5 μm in-plane length

scales) remain essentially unchanged during this transition, suggesting that surface roughness variations are relatively small. At a slightly higher temperature, approximately 360 °C, one observes the emergence of a peak at $2\theta=48.7°$, which is consistent with Pt_3Ge_2(232). This being the only intense peak detected for that phase, it suggests a strong preferential orientation. At 370 °C, three new peaks can be attributed to PtGe. The peaks at $2\theta=36.4°$, 37.7°, and 50.1° are, respectively, indexed as the overlap of the (020) and (111) diffractions, the overlap of (121) and (220), and, finally, (002). At $T_a \approx 380$ °C, even with Pt being not yet completely consumed, we clearly observe that three germanide phases are simultaneously present in the thin film; in particular, Pt_3Ge_2 and PtGe form at about the same temperature. This exceptional behavior—namely, the simultaneous growth of several phases during the annealing treatment—diverges from the observations that phases should form sequentially in thin film systems. This will be further discussed below.

The PtGe phase eventually consumes all others and remains stable until 440 °C, at which point the film completely transforms into Pt_2Ge_3 as evidenced by the large number of diffraction peaks for this low-symmetry phase: (211), (600), (302), (311), (402), (411), (502), (511), (312), (800), (611), (801), (512), and (013). This phase transition is accompanied by a marked increase of the diffuse light scattering signal for the 5 μm in-plane length scale.

Finally, $PtGe_2$ forms at $T_a=510$ °C and remains stable until 800 °C, when the film melts. The $PtGe_2$ (020), (011), (111), (220), (211), (121), and (130) planes can be identified in the XRD data. We note that the 5 μm light scattering signal exhibits another large increase at $T_a=500$ °C. Moreover, the light scattering signal corresponding to a 0.5 μm in-plane correlation length scale also exhibits a small increase at this temperature. During melting, sharp changes in the light scattering are detected for both in-plane length scales.

In summary, five of the six stable phases from the Pt–Ge binary phase diagram were observed in the current thin film annealing experiment. On the basis of the maximum diffracted intensity for each phase, the sequence is Pt_2Ge, Pt_3Ge_2, PtGe, Pt_2Ge_3, and $PtGe_2$, i.e., phases with an increasing amount of Ge form at increasingly higher temperatures. However, it must be pointed out that up to three germanide phases coexist with the initial Pt film during the initial annealing stages. The only stable germanide phase that has not been clearly observed during the thermal ramp is Pt_3Ge. It is possible that the shift of the Pt peak towards lower angular values at $T_a=300$ °C corresponds to the appearance of this phase. However, such a shift could also be related to grain growth or stress within the film, as previously observed during the reaction of, for example, Co with Si.[32]

A. Sensitivity to oxidation

The sensitivity of the deposited metal films to oxidation varies considerably given the range of materials under study. Although the annealing experiments were conducted in purified He with a measured oxygen partial pressure below 1 ppb (parts per billion), a native oxide may have formed on the surface of the deposited metal films as a result of exposure to atmosphere. This provides a source of oxygen atoms which can then drastically alter the thin film reaction. In order to identify possible oxidation-related effects, metal films were also deposited on an inert layer of Si_3N_4. Therefore, any unexpected transformation observed during the annealing of these samples provides strong evidence for surface oxide playing a role.

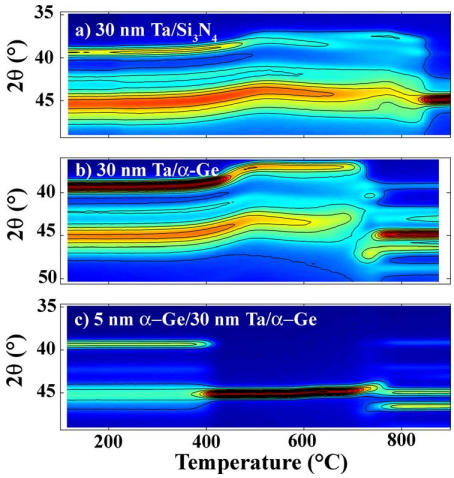

FIG. 2. XRD intensity contour maps ($\lambda=0.1797$ nm, log scale intensity) plotted as a function of annealing temperature T_a during a thermal ramp at 3 °C s^{-1} in purified He for a 30-nm-thick Ta film (a) on Si_3N_4, (b) on α-Ge, and (c) on α-Ge but covered with a 5 nm Ge cap.

The presence of oxygen-related transitions was quite noticeable for Ti, Zr, Hf, V, Nb, Ta, and Mn. As an example, we present in Fig. 2 a comparison of the *in situ* data for 30-nm-thick Ta films prepared in three different configurations: (a) on Si_3N_4, (b) on α-Ge, and (c) on α-Ge but with a 5 nm α-Ge cap. All samples were ramped from 100 to 900 °C at 3 °C s^{-1} in a purified He atmosphere. In Fig. 2(a), the Ta peaks observed at low temperature shift towards higher d spacings (lower 2θ) upon annealing over 400 °C, suggesting the gradual incorporation of an increasing amount of oxygen into the metal lattice. At higher temperatures, the Ta film fully oxidizes, as indicated by the brownish surface color observed following annealing to 900 °C.

When comparing Figs. 2(a) and 2(b), it is clear that similar features can be observed for the Ta film deposited on α-Ge. Above 700 °C, we note the presence of both oxide and germanide peaks, thus creating difficulties in the phase identification. The deposition of a thin α-Ge cap layer directly over the metal film without breaking vacuum in the magnetron sputtering system has proven to be an effective solution for limiting the effects of oxidation during the metal-Ge reactions. In Fig. 2(c), we can clearly see that the Ta peaks remain at their predicted position until the reaction with Ge begins at approximately 710 °C. All peaks in Fig. 2(c) could be identified as tantalum germanides. However, the 5 nmα-Ge did not help for all metal-germanium system

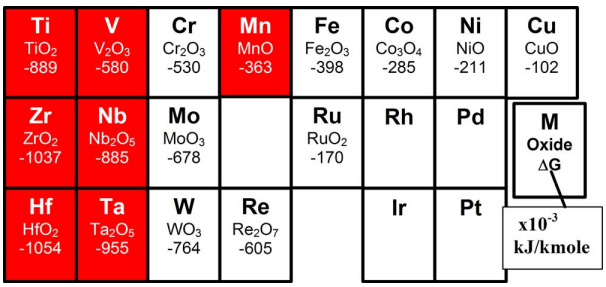

FIG. 3. Free energy of oxide formation for the transition metals at 298 K. Metals exhibiting oxidation problems in this study are highlighted.

affected by oxidation. For example, the $TiGe_2$ phase could not be observed, due to the presence of O at the surface, as evidenced by RBS measurements.

Fortunately, not all metals suffered from this oxidation problem. Similar tests have shown that uncapped films of W, Re, Ni, Pt, Ru, Re, Ir, Cu, and Co are all stable on Si_3N_4 during annealing in purified He up to 1100 °C. Mo, Pd, and Fe exhibited slight signs of oxidation or reaction with Si_3N_4, but only at temperatures above the range of relevance for germanide formation.

The oxidizing behavior is directly related to the free energy of oxide formation per atom of metal.[33] Values at 298 K are presented in Fig. 3 for the most common oxide for a given metal.[34] As expected, metals characterized by the largest difference in free energy (most negative value for the free energy change during oxidation) are most easily oxidized, with W and Mo being notable exceptions.

B. Phase formation sequence

In order to determine the phase formation sequence for each metal-Ge system, experiments identical to those presented above for Pt–Ge were conducted. RBS analyses were carried out on selected quenched samples to obtain direct compositional measurements of the reacted films to confirm and complement phase identification based on *in situ* XRD results. In view of the drastic reduction of oxidation effects resulting from the addition of an α-Ge overlayer, phase identification was carried out on such samples. While one would expect possible differences in the measurement of phases present when reactions can occur at two interfaces instead of one, we note that the sequences measured *in situ* for samples with and without cap layers were not distinguishable for the 14 systems not prone to oxidation.

The analysis of the complete set of results revealed a wide range of behaviors. Figure 4 presents typical XRD results for (a) Zr on Ge(001), (b) Pd on α-Ge, (c) Pd on Ge(001), (d) Ir on Ge(001), and (e) W on Ge(001). The Zr–Ge reaction [Fig. 4(a)] is characterized by the formation of three different phases. It is one of the elements most sensitive to oxidation since the formation of a Zr oxide phase is observed despite the presence of a 5-nm-thick Ge cap layer. Indeed, ZrO_2 becomes detectable in the XRD maps at T_a=550 °C and has completely consumed the $ZrGe_2$ layer when T_a reaches 750 °C. At the same time as the ZrO_2 phase grows, the

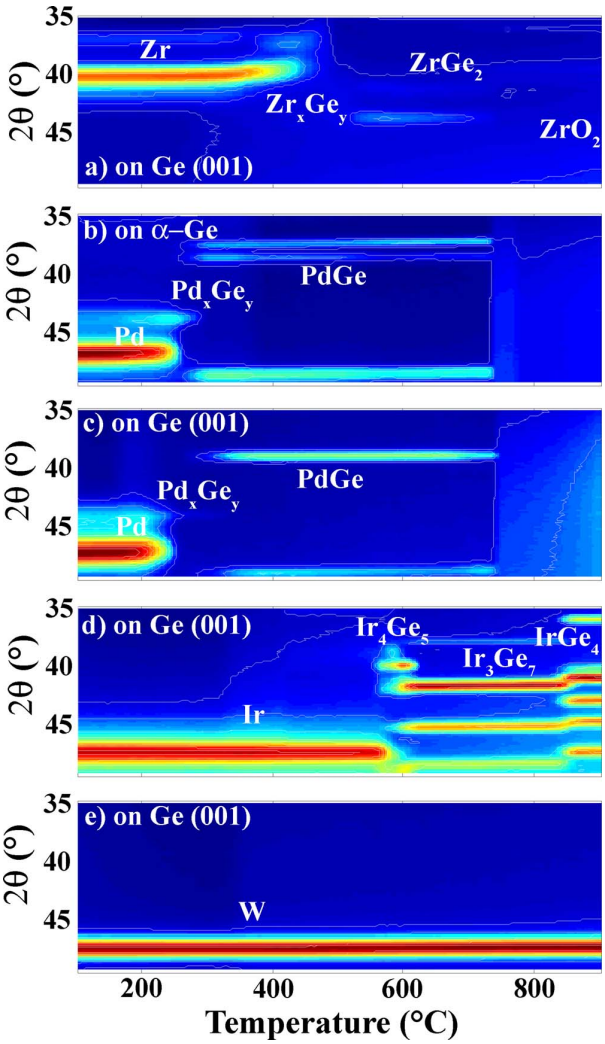

FIG. 4. XRD intensity contour maps (λ=0.1797 nm, log scale intensity) plotted as a function of annealing temperature T_a during a thermal ramp at 3 °C s^{-1} in purified He for 30-nm-thick metal films on Ge: (a) Zr on Ge(001), (b) Pd on α-Ge, (c) Pd on Ge(001), (d) Ir on Ge(001), and (e) W on Ge(001). Films were capped with a 5-nm-thick α-Ge overlayer to prevent oxidation.

Ge(220) peak grows at 53.4° indicating the separation of Zr and Ge. The reaction with Pd was found to begin at the lowest temperature of all systems investigated [Figs. 4(b) and 4(c)]. The most interesting phase for contacts, PdGe, is present from 330 to 740 °C, when it melts. However, the resistance and light scattering measurements (not shown) indicate severe morphological degradation of this phase at temperatures as low as 550 °C. While the reaction on both Ge(001) and α-Ge reveals the same initial features, different film textures develop as the reaction progresses. As discussed below, the data in Figs. 4(b) and 4(c) clearly indicate that the PdGe(210) peak is only observed on α-Ge. The reaction of Ir with Ge [Fig. 4(d)] also leads to the formation of three phases, the latter being the richest in Ge of all phases iden-

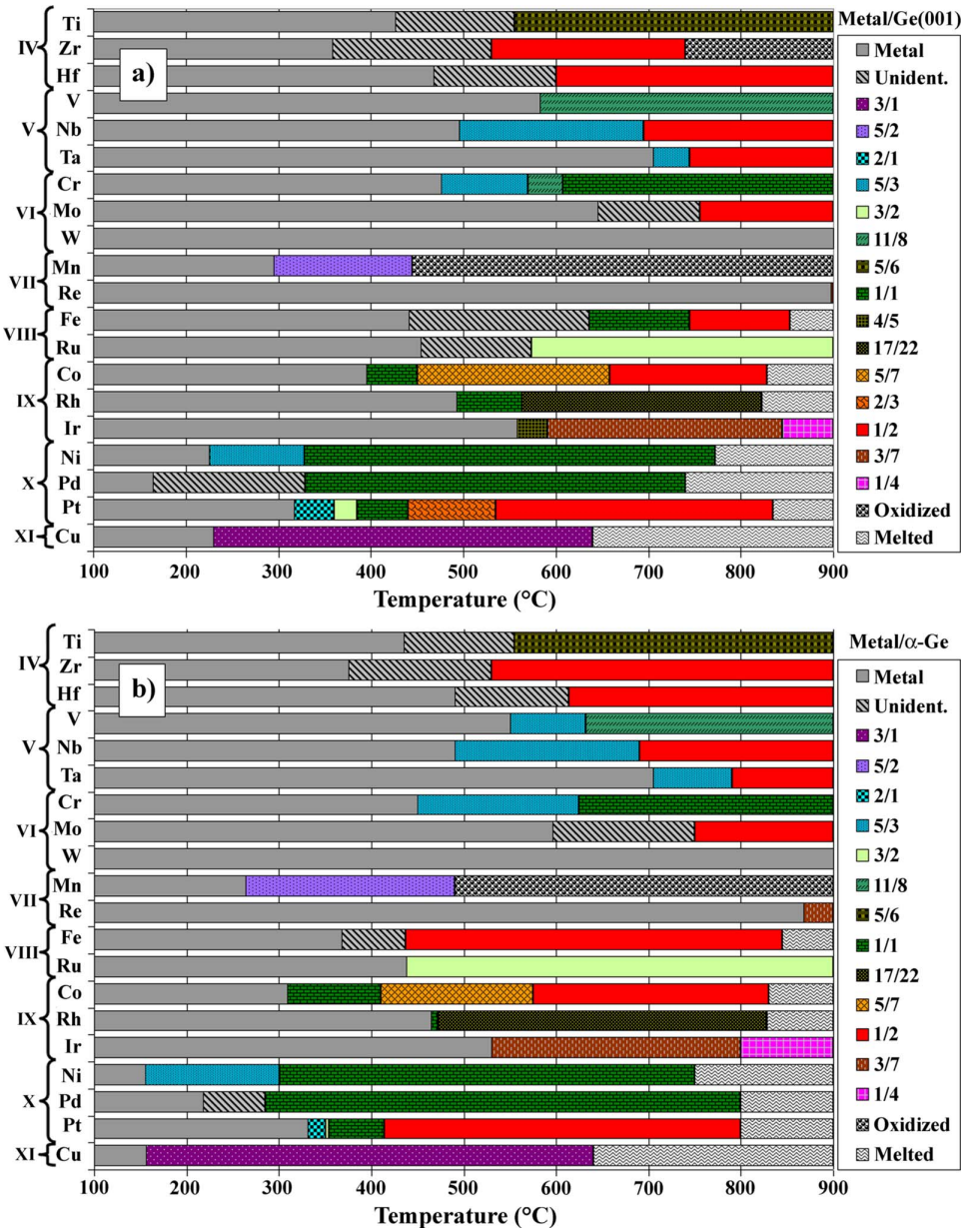

FIG. 5. Phase sequence of the reaction of 30-nm-thick transition metal films capped with a 5-nm-thick α-Ge overlayer deposited on (a) Ge(001) and (b) α-Ge during a 3 °C s^{-1} ramp anneal in purified He. Metal to germanium ratios in each germanide phase are indicated in the color-coded legend.

tified in this study ($IrGe_4$). The annealing of W on Ge(001) at temperatures up to 900 °C did not lead to the formation of any germanide phase [Fig. 4(e)].

Schematic overviews of the phase formation sequence for each metal on Ge(001) and α-Ge are presented in Figs. 5(a) and 5(b), respectively. When there is an overlap between different phases, the phase with the strongest XRD intensity is indicated. In rare occasions, some phases could not be identified unambiguously because of the small number of XRD peaks present in the measured 2θ windows. This mostly occurred at low temperature in a regime where several metal-rich, low-symmetry phases coexist with the pure metal layer. Still, all potentially interesting phases with respect to our selection criteria as contacting materials were successfully identified.

The summary plots are ordered by families of the Periodic Table; phases are classified by their proportion of metal and Ge. The first two families (IV and V) are the most susceptible to oxidation. They form germanides at relatively high temperatures and, despite the presence of the Ge cap, are not totally exempt of oxidation. Even though Mn is a group VII element, it appears to be the most reactive film with oxygen. In fact, the formation of an oxide is observed at temperatures as low as 445 °C. Only one metal, W, did not form any

detectable phases, even at the highest temperature investigated, whereas Re and Mo completely reacted only above 750 °C. Transition metals on the right-hand side of the Periodic Table reacted with Ge at the lowest temperatures, a characteristic that is consistent with the low melting points of these metals. The low melting points and the rapid atomic diffusion even at low temperature allow for the early formation of germanide phases. They, however, also result in an undesirable early thermal degradation of the films that may require much optimization work if such contact materials are to be integrated in large scale production schemes.

Differences in formation temperatures and, in some cases, in the phase sequence were observed when the substrate was changed from crystalline to amorphous Ge. In general, Ge rich phases appeared at lower temperature on amorphous than single crystal substrates. For example, the formation of $FeGe_2$ is lowered from 745 °C on Ge(001) to 408 °C on α–Ge. The decrease in formation temperature and the variation in the sequence may have multiple origins. From a kinetics point of view, the crystallinity of the substrate affects the diffusion paths and coefficients. The crystallinity sometimes also offers a low energy interface that may play a role. More importantly, at high temperature, the variation in free energy which drives the reaction becomes small since many phases have already formed. As a result, the formation of the phase with the highest Ge fraction often becomes nucleation limited. In this case, the crystallization energy is often sufficient to lower the barrier in such a way that nucleation is not an issue.

C. Sheet resistance

As the present work is aimed at identifying appropriate materials for contacting Ge-based devices, interesting candidates must exhibit a low resistance, be formed at a reasonably low temperature, and remain morphologically and thermodynamically stable over a wide range of temperatures. Because of differences in resistivity between the various germanide phases and the expanding thickness of the film resulting from Ge incorporation as the reaction progresses, phase formation can lead to abrupt changes in the sheet resistance measured *in situ* during annealing. Morphological degradation at high temperature also leads to increases in sheet resistance, during which the XRD data exhibit little or no variation.

The real-time resistance measurements during annealing were carried out on thin (200 nm) α-Ge layers on an insulating substrate composed of SiO_2 on Si(001). Indeed, the use of a thick Ge(001) substrate is not possible for these measurements since it becomes conductive at high temperature as electrons populate the conduction bands of the semiconductor. In these conditions, the resistance signal would be completely dominated by the substrate behavior [see, for example, Fig. 1(a)]. The α-Ge/SiO_2/Si(001) substrate also has the advantage of withstanding higher temperatures than bulk Ge, thus extending the range of annealing conditions to temperatures higher than the melting point of Ge.

The overall set of results is plotted as a function of T_a in

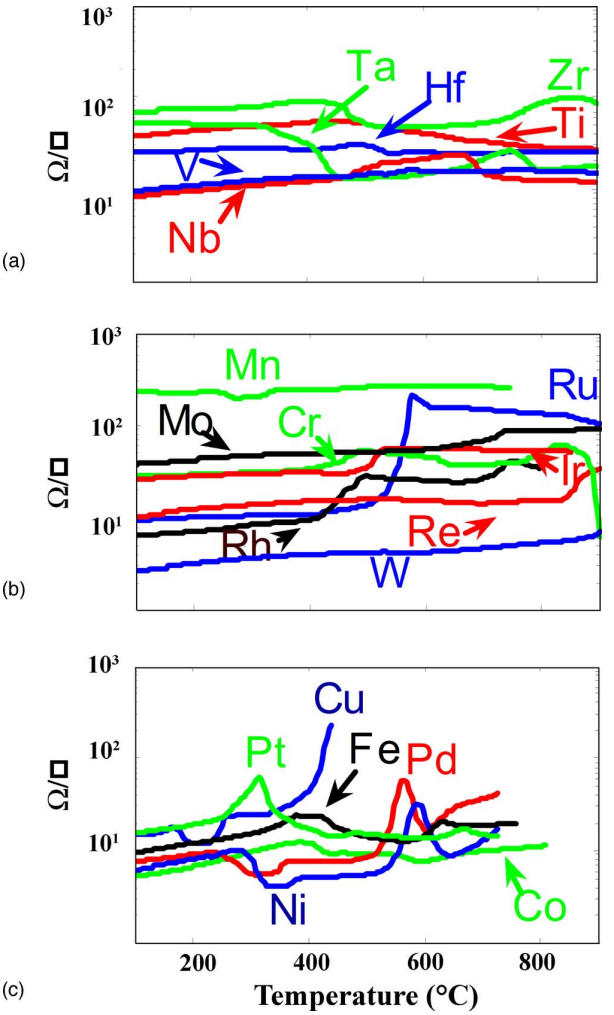

FIG. 6. Sheet resistance, plotted as a function of annealing temperature T_a, during a thermal ramp at 3 °C s^{-1} in purified He for 30-nm-thick metal films capped with 5 nm α-Ge. (a) Metals prone to oxidation: Ti, Zr, Hf, V, Nb, and Ta; (b) metals forming high-resistivity germanide phases: Cr, Mo, Mn, Ru, Rh, and Ir, or exhibiting little reaction: W; and (c) metals reacting at low temperature: Fe, Co, Ni, Pd, Pt, and Cu.

Fig. 6. Data acquired in the *in situ* setup have been normalized using values from *ex situ* four point probe measurements (linear configuration) performed on samples before the anneals. Sheet resistance curves for a first group of metals reacting with Ge at low temperature but also exhibiting severe oxidation (Ti, Zr, Hf, V, Nb, and Ta) are shown in Fig. 6(a). For these systems, most of the high temperature phases exhibit severe surface roughening ($HfGe_2$, $NbGe_2$, and $TaGe_2$), as indicated by complementary light scattering measurement (not shown). The sheet resistance values obtained range from 18 to 85 Ω/□. We note, however, that some phases could potentially exhibit lower values with a better control of film oxidation by optimizing the cap-layer quality.

Other metals such as Cr, Mo, Mn, Ru, Rh, Ir, and Re react with Ge to form germanide phases with sheet resistance values at least as high as those for the metal film itself [Fig. 6(b)]. Also, as mentioned earlier, no reaction could be de-

TABLE I. Sheet resistance of quenched phases on α-Ge obtained during 3 °C s^{-1} ramp anneals in He.

Germanide	Sheet resistance (Ω/□)	T_a (°C)	Germanide	Sheet resistance (Ω/□)	T_a (°C)
Co+CoGe	9.9	360	$Pd+Pd_xGe_y$	7.3	251
$Co_5Ge_7+CoGe_2$	6.3	520	PdGe	4.4	340
$CoGe_2$	5.5	650	$Pt+Pt_3Ge$	16	300
Co_2Ge	7.2	430	Pt_2Ge	8.7	350
Cr_5Ge_3	23	480	Pt_3Ge_2+PtGe	6.9	375
Cr_5Ge_3	51	560	PtGe	6.3	390
CrGe	26	670	$PtGe_2$	4.2	450
Cu_3Ge	8.5	225	$PtGe_2$	6.7	720
FeGe or Fe_5Ge_6	26	390	$PtGe_2$	11	807
FeGe or Fe_5Ge_6	28	440	Re_3Ge_7	81	925
$FeGe_2$	14	580	Rh+RhGe	10	440
Hf_xGe_y+Hf	26	470	RhGe	21	480
Hf_xGe_y	24	545	$Rh_{17}Ge_{22}$	32	600
$Ir+Ir_4Ge_5$	7.0	260	$Ru+Ru_2Ge_3$	30	560
$Ir+Ir_4Ge_5$	7.2	460	Ru_2Ge_3	3800	700
Ir_3Ge_7	11	580	Ru_2Ge_3	2800	925
Mn_5Ge_2	180	284	$TaGe_2$	18	780
Mn_5Ge_2	160	320	$Ti+Ti_xGe_y$	63	480
MnO	710	520	Ti_5Ge_6	58	760
$Mo_{13}Ge_{23}$	18	720	Ti_5Ge_6	120	925
$Nb+Nb_5Ge_3$	20	600	$V+V_xGe_y$	18	500
$NbGe_2$	30	680	V_5Ge_3	32	600
$Ni+NiGe+Ni_5Ge_3$	7.7	250	$Zr+Zr_xGe_y$	110	360
$NiGe+Ni_5Ge_3$	8.5	270	$Zr+Zr_xGe_y$	62	460
$NiGe+Ni_5Ge_3$	10	285	Zr_xGe_y	110	620
$NiGe+Ni_5Ge_3$	5.0	315	$ZrGe_2$	85	760
NiGe	3.1	380	$ZrGe_2+ZrO_2$	190	925

tected by XRD for W within the temperature range studied. The sheet resistance curve for this system remains quite stable through the annealing process, displaying only a slow steady increase typical of a metallic material [Fig. 6(b)].

Finally, some metals react with Ge to form low resistivity germanide phases [Fig. 6(c)]. This last group (Fe, Co, Ni, Pd, Pt, and Cu) includes the most promising candidates for contacting Ge using a straightforward process. Among those, NiGe and PdGe phases appear especially interesting: they exhibit the lowest sheet resistance, form at low temperature (150 and 360 °C, respectively), and remain stable over a wide temperature range. The morphological degradation (agglomeration) begins at 580 and 550 °C for NiGe and PdGe, respectively, during a 3 °C s^{-1} ramp rate. The respective increase in sheet resistance at 380 and 350 °C correlates with the increase in roughness induced by the crystallization of α-Ge. This phenomenon would of course not occur in the source and drain regions of devices built on single crystal germanium.

We are interested here in the detection of low resistance phases and many of the curves presented in Fig. 6 show low resistance values at high temperatures. The low resistance can of course not only be the result of the formation of a low resistivity "metallic-type" phase but could also originate from the formation of a semiconducting germanide that becomes very conducting at high temperatures. To obtain quantitative values of the sheet resistance for the different germanide phases at room temperature, samples were prepared by heating metal films on α-Ge up to the appropriate temperature for a given phase, followed by rapid cooling. XRD scans were performed immediately after quenching to confirm the presence of the desired phase.

The room-temperature sheet resistances measured for all quenched phases are given in Table I. The sheet resistance of any germanide phase always corresponds to a fixed initial metal thickness. As a result, if two phases have similar resistivities, the films containing more Ge will typically exhibit lower sheet resistances since the thickness of the transformed

TABLE II. Resistivity of selected metal germanide phases formed on α-Ge.

	Sheet resistance (Ω/□)	Nominal thickness (nm)	Resistivity ($\mu\Omega$ cm)
NiGe	3.1	71	22
Cu_3Ge	8.5	28	24
PdGe	4.4	68	30
PtGe	5.2	71	44
$PtGe_2$	4.2	113	48
$CoGe_2$	5.5	125	69

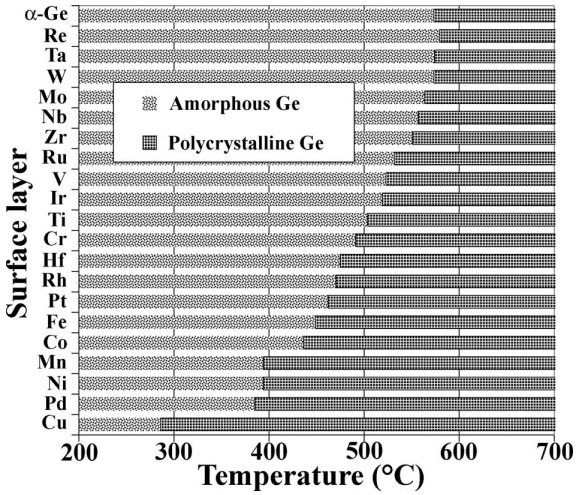

FIG. 7. Effect of a 30-nm-thick metal overlayer on the crystallization temperature of a 200-nm-thick α-Ge layer on a $SiO_2/Si(001)$ substrate during a thermal ramp at 3 °C s^{-1} in purified He.

films generally increases with Ge content. For example, even if the PdGe phase displays a lower bulk resistivity than the $PtGe_2$ phase, PdGe films exhibit a higher sheet resistance since the film is thinner at that stage of the reaction.

Resistivity values ρ based on expected thicknesses using known film densities or crystal structures were calculated from the sheet resistance data for selected low resistivity phase (Table II). We note that resistivity values for NiGe (ρ=22 $\mu\Omega$ cm) and PdGe (ρ=30 $\mu\Omega$ cm) approach those of silicides currently used in microelectronics circuits (10 $\mu\Omega$ cm for NiSi and 15 $\mu\Omega$ cm for $CoSi_2$)[35] even though the crystallization of the amorphous substrates leads to rougher films and increases in resistance.

D. Germanium crystallization

Metal-induced (or metal enhanced) crystallization of amorphous silicon has attracted a lot of attention for applications in solar cells and thin film transistors. A similar phenomenon is observed for the crystallization of α-Ge in the presence of a thin metal layer. Crystallization is monitored in our *in situ* experiments by the appearance of the Ge(220) XRD peak which is accompanied by a significant decrease of the background signal. It is also noticeable in the resistance and light scattering signals as mentioned earlier. Uncapped samples were used for this comparative study, in order to have a single layer of α-Ge and to eliminate a possible contribution of the capping layer. The results are summarized in Fig. 7. The metals that formed germanides at the lowest temperatures—Cu, Ni, Pd, Mn, and Co—also gave rise to the most significant reduction in the crystallization temperature of α-Ge.

E. Anisotropic thermal expansion

It has been recently reported that some silicide phases exhibit strongly anisotropic thermal expansion coefficients.[36,37] Our *in situ* XRD data suggest a similar behavior for a number of germanide phases. For example, the $PtGe_2$(121) peak position (2θ=55° on Fig. 1) shifts towards lower 2θ values for increasing temperature while the (130) peak from the same phase (2θ=58°) is displaced in the opposite direction. Similar observations of a negative thermal expansion were made for $Ge_{22}Rh_{17}$ and NiGe. All other phases exhibit a positive thermal expansion with, in some cases, a significant anisotropy. For example, all peaks from the Ir_3Ge_7 shift by 0.1° towards lower angles (larger d spacings) when T_a increases from 650 to 800 °C, whereas the PdGe (111) and (211) peaks shift by 0.1° and 0.3°, respectively, between 350 and 700 °C.

IV. DISCUSSION

The thermally induced reactions of 20 transition metals with Ge were investigated using *in situ* synchrotron XRD, diffuse light scattering, and resistance measurements complemented by selected *ex situ* RBS analyses. This enabled the identification of the crystalline phases formed during the thin film reaction, and provided information regarding the temperature range over which given germanide phases exist.

A. Phase formation sequence

As indicated in the Introduction, phase formation sequences are typically determined using anneal-and-quench experiments in which the temperature interval between measurements is of the order of 25 °C or more. Furthermore, the nature of the substrate, the film thickness, and the annealing conditions vary considerably in these investigations. It is therefore not surprising that different phase sequences have been reported in the literature. It is also clear from the results presented in Sec. III that several phases are detected only over relatively short temperature windows. Moreover, as observed for the Pt–Ge system in Fig. 1, many phases can coexist. This can certainly explain that some phases could have been inadvertently missed in anneal-and-quench experiments.

Our *in situ* study has the advantage of providing a continuous observation of phases present in the film. The very high intensity probe beam also enables us to detect phases that are present in minute quantities. In order to facilitate their observation, we note here that all x-ray maps were plotted on a logarithmic intensity scale to cover the largest possible dynamic range in detected intensities. This additional sensitivity has helped us to reveal the coexistence of more than one phase in some temperature ranges.

Many dissimilarities observed between the different phase sequences reported in the literature and our *in situ* results concern the formation of the first phase. As this depends to a large extent on the microstructure of the metal films, differences at this stage are therefore not that uncommon nor surprising. However, phases usually grow sequentially during thin film reactions, meaning that only one phase would grow at the expense of another at a given time. The simultaneous growth of Pt_3Ge_2 and PtGe, while both Pt_2Ge and Pt are still present, departs from this usual behavior. Although typically

not observed for thin film reactions, this phenomenon was also noted for Ta and Ni films both on α-Ge and Ge(001), Fe and Co films on α-Ge, and Ir films on Ge(001). While the coexistence of many phases is clear in the Ta system, the presence of the Ge cap layer as a contributor cannot be ruled out since the uncapped film showed drastically different behaviors. The simultaneous growths of Ni on Ge substrates were also very recently described in a doctoral dissertation[38] in which the diffracted x-ray intensities of Ni_5Ge_3 and NiGe, monitored *in situ* during the anneal, were shown to follow the $t^{1/2}$ dependence expected for a growth controlled by diffusion. This behavior is similar to what is observed in bulk diffusion couples for which the dimensions are much larger and the annealing time much longer. In bulk samples after long anneals, all the phases stable at the temperature selected for the experiment are expected to grow simultaneously (after critical thicknesses are reached) in a diffusion controlled regime. The difference with thin film reactions in which the phase typically grows sequentially has been attributed to the reduced dimensions, the shorter time scales, and lower temperature as well as the larger importance of interface and surface energies and reaction rates at these interfaces. The discovery of simultaneous growth in thin film therefore suggests that for some of the metal-Ge systems, with films of metals of only 30 nm in thickness, diffusion is controlling the growth from the early stages. Thus these thin film samples behave similarly to bulk diffusion couples after long anneals. While this phenomenon is not understood at present and its origins may depend on multiple factors, the diffusion limited growth must be linked with fast reaction rates at interfaces. Moreover, to get simultaneous growth, one must expect that the diffusion coefficient of the most mobile species should be of the same order in each of the growing phases (supposing that the free energy changes are similar at each growing interface).

Our XRD experiments also revealed significant differences in film texture as the relative peak intensities vary greatly for amorphous and single crystal substrates. Consider the reaction of Pd with Ge as an example. At low temperature, the films appear relatively similar on both substrates, being characterized by an intense Pd peak and a weak peak from a Pd-rich phase that might have formed during deposition. The latter phase increases in intensity as the film is heated up. A first difference is noted when a broad peak emerges only on Ge(001). Thereafter, PdGe forms with different textures on the two substrates. A similar behavior was observed in the case of 14 of the 20 metals investigated—Hf, V, Cr, Mo, Mn, Re, Fe, Co, Rh, Ir, Ni, Pd, Pt, and Cu. Polycrystalline films grown on single crystal substrates are expected to show a texture that is relatively random since a very few phases allow an epitaxial alignment with the underlying substrate. Our observations are inconsistent with this expected behavior and certainly imply that some grain orientations provide lower interface energies with the single crystal substrate. While the epitaxial alignment is not generally expected, it is possible that these low energy interfaces be related to plane alignment across the interface (axiotaxy), as was observed for many silicides.[39–41]

B. Best candidates for Ge-based microelectronic circuits

Among the different germanides studied, we identified six metals that formed low resistivity phases (Fe, Cu, Co, Pt, Pd and Ni), each one having advantages and limitations with respect to a complementary metal-oxide semiconductor (CMOS) device processing technology.

The reaction of Fe with Ge leads to the formation of the low resistivity phase $FeGe_2$. The measured resistivity (129 $\mu\Omega$ cm) is, unfortunately, not as low as those observed for the other selected materials. Furthermore, the phase formed only at high temperature on Ge(001) (745 °C), a temperature too close to the melting point of Ge (938 °C), to allow for a reasonable process window.

Copper and Ge react at extremely low temperature (155 °C). However, as a result of the fast diffusion, the germanide film degrades morphologically at temperatures of only 350 °C during a ramp annealing at 3 °C s^{-1}. This degradation temperature is clearly too low for the processing of both interconnects and low-*k* dielectrics, which currently require the equivalent of nearly 400 °C for several hours. Although the Cu_3Ge resistivity is quite low (24 $\mu\Omega$ cm), a process involving Cu in direct contact with the active semiconductor would surely face many hurdles in a production environment sensitive to contamination.

The Co–Ge system exhibits two phases that are potentially useful for contacting Ge:Co_5Ge_7 and $CoGe_2$ (ρ =69 $\mu\Omega$ cm). Co_5Ge_7 forms at 450 °C and remains stable up to 660 °C under our typical 3 °C s^{-1} ramp. At this temperature, the nucleation controlled formation of $CoGe_2$ leads to a significant increase in roughness. While $CoGe_2$ is preferred for its resistivity and thermal stability, Co_5Ge_7 shows a clear advantage in terms of film roughness.

Three of the platinum germanide phases are of interest for microelectronics—PtGe (44 $\mu\Omega$ cm), Pt_2Ge_3, and $PtGe_2$ (48 $\mu\Omega$ cm). The first two are present over a temperature range of less than 100 °C, below 500 °C, on Ge(001). Since the formation temperature is expected to depend significantly on dopants, such a small process window severely limits possibilities for integration. $PtGe_2$ is morphologically stable over a much larger temperature range: 500–700 °C. However, the formation of this phase triggers a large increase in film roughness.

The reaction of Pd with Ge leads to the formation of PdGe, a phase that forms at low temperature and is stable over a wide range of temperatures (280–800 °C). Its resistivity of 30 $\mu\Omega$ cm is among the lowest observed. The most important drawback is that morphological degradation of the film is observed at only 530 °C on α-Ge and at 600 °C on Ge(001) during ramp anneals at 3 °C s^{-1}. Still, thermal stability to this temperature may be sufficient for processing; this germanide film may be a potential solution for Ge-based microelectronics.

Similarly to Pd, Ni reacts with Ge to form a monogermanide that is stable over a wide range of temperatures (300–760 °C) and exhibits the lowest resistivity (22 $\mu\Omega$ cm). The morphological degradation could again become a limiting factor: 540 °C on α-Ge and 600 °C on Ge(001) during ramp anneal at 3 °C s^{-1}.

Many elements showed important oxidation (Ti, Zr, Hf, V, Nb, and Ta) upon annealing. While this behavior is not desirable for the application at hand, it can certainly be controlled as C54–$TiSi_2$ contacts have been used extensively in Si-CMOS devices. As an example, low resistivity $TiGe_2$ has been observed to form by other studies that achieved a better control on oxidation.[11–13] However, the higher formation temperatures necessary to reach the low resistivity phases may still be detrimental to the stability of Ge-CMOS devices.

C. Crystallization of α-Ge

Metal-induced crystallization of α-Si has been studied extensively.[42–44] An increased metal concentration at grain boundaries during the crystallization process leads to the formation of a metal silicide at these interfaces. For the Ni–Si system, the Ni chemical potential is lower at the $NiSi_2$/α-Si interface, whereas that for Si atoms is lower at the $NiSi_2$/*c*-Si interface.[43] Furthermore, Si diffusion is much faster in the silicide than in silicon. Consequently, Si atoms are driven, through the interfacial silicide, from the amorphous to the crystalline side of the boundary, therefore leading to rapid polycrystalline grain growth.

The present study clearly demonstrates that most metals lower the crystallization temperature of α-Ge. In all cases where the crystallization temperature is reduced, it is clear that a germanide phase has formed *before* the onset of α-Ge crystallization. This supports the model described above which requires the presence of a germanide phase for the lower temperature crystallization to occur, the reason being that Ge diffuses much faster in a germanide than in Ge itself. We propose that the temperature at which crystallization occurs depends primarily on the ease at which a germanide can form (reaction rate and metal diffusion in the growing germanide) and secondly on the ability of this germanide to enhance crystallization of Ge through fast Ge diffusion within this already formed germanide. One should note here, however, that while this interpretation favors the presence of the germanide, the presence of Au on Si also helps the recrystallization without the possibility of forming a silicide.

V. CONCLUSION

The aim of the present study was to complete a systematic investigation of metal-germanium reactions to isolate promising candidates for contacting Ge-based microelectronic devices. The classification of the metals presented here also allows for the selection of materials for various applications involving Ge. Films could be selected on the basis of their roughness and resistance (low or high) as well as on formation temperature, degradation, and texture.

Based on their low formation temperature, low resistivity, limited film roughness, sufficient morphological stability, and limited sensitivity to oxidation, NiGe and PdGe were found to be the most promising candidates. Other materials such as PtGe, $PtGe_2$, and $CoGe_2$ are also potentially interesting materials for contacting applications. All these are, however, subject to low temperature thermal degradation; therefore, they would probably require stabilization through alloying. With optimization of the capping layer, one could also try to diminish the oxidation of the metals from the left-hand side of the Periodic Table, since germanides formed from these metals are more likely to endure a higher thermal budget. This higher morphological stability is also linked with a higher formation temperature that may, however, be detrimental to Ge-CMOS devices.

Although focused on the contact properties, this study is relevant to other applications involving germanides or germanosilicides. As an example, the fabrication of thin film transistors relies on the crystallization of amorphous layers. Through this study, we surveyed the effect of several metals on the crystallization of α-Ge. The crystallization of germanium during a 3 °C s^{-1} anneal can be lowered from 570 down to 290 °C. The most efficient materials are Cu, Pd, Ni, and Mn. It is also interesting that three of the germanides studied showed strongly anisotropic thermal expansion: NiGe, $PtGe_2$, and $Rh_{17}Ge_{22}$.

Finally, simultaneous growth of multiple phases was observed for Ni, Pt, Co, Ir, Fe, and possibly Ta films on Ge substrates. In thin films, it is believed that the reduced dimensions, the variations in growth kinetics for each phase, as well as the importance of interfaces and nucleation typically lead to sequential growth. Our results suggests that in these systems, diffusion takes a predominant importance as for bulk diffusion couples in which phases grow simultaneously after long anneal times. In these metal-Ge systems, the behavior observed may suggest that the diffusion is more limiting than the effects at interfaces.

ACKNOWLEDGMENTS

The authors thank Roy Carruthers of IBM Research for film deposition and Dr. Jean Jordan-Sweet for her assistance at the X20 beamline at the NSLS. The authors are indebted to Francois d'Heurle from IBM Research for a thorough review of this manuscript. This work was in part supported by the Natural Sciences and Engineering Council of Canada (NSERC) and the Canada Research Chair program. The research was carried in part at the National Synchrotron Light Source, Brookhaven National Laboratory, which is supported by the U.S. Department of Energy, Division of Materials Sciences and Division of Chemical Sciences, under Contract No. DE-AC02-98CH10886.

[1]J. D. Cressler, IEEE Trans. Microwave Theory Tech. **46**, 572 (1998).
[2]D. L. Harame *et al.*, Appl. Surf. Sci. **224**, 9 (2004).
[3]W. Lu, S. J. Koester, X.-W. Wang, J. O. Chu, T.-P. Ma, and I. Adesida, J. Vac. Sci. Technol. B **18**, 3488 (2000).
[4]A. Notargiacomo, L. Di Gaspare, G. Scappucci, G. Mariottini, E. Giovine, R. Leoni, and F. Evangelisti, Mater. Sci. Eng., C **23**, 671 (2003).

[5]S. Kanjanachuchai, Semicond. Sci. Technol. **14**, 1065 (1999).
[6]D. J. Paul, Thin Solid Films **321**, 172 (1998).
[7]G. Ribes, J. Mitard, M. Denais, S. Bruyere, F. Monsieur, C. Parthasarathy, E. Vincent, and G. Ghibaudo, IEEE Trans. Device Mater. Reliab. **5**, 5 (2005).
[8]H. Shang *et al.*, IEEE International Electron Device Meet. **441**, 17.4.1 (2002).
[9]V. G. Samsonov and V. N. Bondarev, *Germanides* (Primary Source, New York, 1970), p. 233.
[10]*Handbook of Binary Alloy Phase Diagrams* (CD Version 1.0) (ASM International, 1996).
[11]S. P. Ashburn, M. C. Ozturk, and J. J. Wortman, J. Electron. Mater. **21**, 81 (1992).
[12]O. Thomas, F. M. d'Heurle, S. Delage, and G. Scilla, Appl. Surf. Sci. **38**, 27 (1989).
[13]O. Thomas, S. Delage, F. M. d'Heurle, and G. Scilla, Appl. Phys. Lett. **54**, 27 (1989).
[14]E. D. Marshall, C. S. Wu, C. S. Pai, D. M. Scott, and S. S. Lau, *Thin Films: The Relationship of Structure to Properties*, MRS Symposia-Proceeding (Materials Research Society, Pittsburgh, PA, 1985), pp. 161–166.
[15]Y. F. Hsieh, L. J. Chen, L. J. Marshall, and S. S. Lau, Appl. Phys. Lett. **51**, 1588 (1987).
[16]M. Wittmer, M. A. Nicolet, and J. W. Mayer, Thin Solid Films **42**, 51 (1977).
[17]I. Goldfarb and G. A. D. Briggs, J. Mater. Res. **16**, 744 (2001).
[18]S. P. Ashburn, M. C. Öztürk, G. Harris, and D. M. Maher, J. Appl. Phys. **74**, 4455 (1993).
[19]J. K. Patterson, B. J. Park, K. Ritley, H. Z. Xiao, L. H. Allen, and A. Rockett, Thin Solid Films **253**, 456 (1977).
[20]S.-L. Hsu, C.-H. Chien, M.-J. Yang, R.-H. Huang, C.-C. Leu, S.-W. Shen, and T.-H. Yang, Appl. Phys. Lett. **86**, 251906 (2005).
[21]J. Y. Spann, R. A. Anderson, T. J. Thornton, G. Harris, S. G. Thomas, and C. Tracy, IEEE Electron Device Lett. **26**, 151 (2005).
[22]G. Ottaviani, C. Canali, G. Ferrari, R. Ferrari, G. Majni, M. Prudenziati, and S. S. Lau, Thin Solid Films **47**, 187 (1977).
[23]Y. F. Hsieh and L. J. Chen, Thin Solid Films **162**, 295 (1988).
[24]Y. F. Hsieh and L. J. Chen, J. Appl. Phys. **63**, 1177 (1988).
[25]M. G. Grimaldi, L. Wielunski, and M.-A. Nicolet, Thin Solid Films **81**, 207 (1981).
[26]M. W. Ruckman, M. del Giudice, and J. H. Weaver, Phys. Rev. B **32**, 1077 (1985).
[27]N. Lundberg, M. Oestling, and F. M. d'Heurle, Appl. Surf. Sci. **53**, 126 (1991).
[28]O. M. Ndwandwe, C. C. Theron, T. K. Marais, and R. Pretorius, J. Mater. Res. **18**, 1900 (2003).
[29]L. Krusin-Elbaum and M. O. Aboelfotoh, Appl. Phys. Lett. **58**, 1341 (1991).
[30]F. M. d'Heurle and J. Gupta, Appl. Surf. Sci. **73**, 214 (1993).
[31]L. R. Doolittle, Nucl. Instrum. Methods Phys. Res. B **9**, 344 (1985).
[32]C. Cabral Jr., K. Barmak, J. Gupta, L. A. Clevenger, B. Arcott, D. A. Smith, and J. M. E. Harper, J. Vac. Sci. Technol. A **11**, 1435 (1993).
[33]G. V. Samsonov, *The Oxide Handbook*, 2nd ed. (IFI/Plenum, New York, 1982).
[34]J. Bénard, *Oxidation des Métaux* (Gauthiers-Villars, Paris, 1964), Vol. 2.
[35]U. Gottlieb, F. Nava, M. Afftonte, O. Laborde, and R. Madar, *Properties of Metal Silicides*, 1st ed. (Inspec, Leuven, Belgium, 1995), Vol. 1, Chap. 5, pp. 191–192.
[36]C. Detavernier, C. Lavoie, and F. M. d'Heurle, J. Appl. Phys. **93**, 2510 (2003).
[37]S. M. Barmin and A. A. Frolov, Fiz. Tverd. Tela (S.-Peterburg) **32**, 1535 (1990).
[38]F. Nemouchi, *Reactivite de Films Nanométrique de Nickel sur Subtrats Silicium-Germanium* (Université Paul Cezanne Aix-Marseille III, Faculté des Sciences et Techniques de Saint-Jerôme, 2005).
[39]C. Detavernier, A. S. Ä. Ozcan, J. Jordan-Sweet, E. A. Stach, J. Tersoff, F. M. Ross, and C. Lavoie, Nature (London) **426**, 641 (2003).
[40]C. Detavernier, C. Lavoie, J. Jordan-Sweet, and A. S. Ozcan, Phys. Rev. B **69**, 174106 (2004).
[41]C. Detavernier and C. Lavoie, Appl. Phys. Lett. **84**, 3549 (2004).
[42]C. F. Cheng, V. M. C. Poon, C. W. Kok, and M. Chan, IEEE Trans. Electron Devices **50**, 1467 (2003).
[43]A. R. Joshi, T. Krishnamohan, and K. C. Saraswat, J. Appl. Phys. **93**, 175 (2003).
[44]M. Wong, Z. Jin, G. A. Bhat, P. C. Wong, and H. S. Kwok, IEEE Trans. Electron Devices **47**, 1061 (2000).